Changes of Nonlinearity and Stability of Streamflow Recession Characteristics under Climate Warming in a Large Glaciated Basin of the Tibetan Plateau

Jiarong Wang[1, 2], Xi Chen[1, 2]*, Man Gao[1], Qi Hu[3], and Jintao Liu[2]

[1] Institute of Surface-Earth System Science, School of Earth System Science, Tianjin University, Tianjin 300072, P.R. China
[2] College of Hydrology and Water Resources, Hohai University, Nanjing 210098, P.R. China
[3] School of Natural Resources and Department of Earth and Atmospheric Sciences, University of Nebraska-Lincoln, Lincoln NE 68583 U.S.A.

***Correspondence to:** Xi Chen, e-mail: xichen@hhu.edu.cn

Abstract. The accelerated climate warming in the Tibetan Plateau after 1997 has profound consequences in hydrology, geography, and social wellbeing. In hydrology, the change of streamflow as a result of changes of dynamic water storage originated from glacier melt and permafrost thawing in the warming climate directly affects the available water resources for societies of the most populated nations in the world. In this study, annual streamflow recession characteristics are analyzed using daily climate and hydrological data during 1980–2015 in the Yarlung-Zangpo River basin (YRB) of south Tibetan Plateau. The recession characteristics are examined in terms of $dQ/dt = -aQ^b$ and the response/sensitivity of streamflow to changes of groundwater storage. Major results show that climate warming has significantly increased the nonlinearity of the response (b) and streamflow stability [$\log(a)$] in most sub-basins of YRB. These changes of recession characteristics are attributed to opposite effects of increases of available water storage and recession timescale on the recession. Climate warming has increased sub-basin water storage considerably by more recharge from accelerated glacier melting and permafrost thawing after 1997. Meanwhile, the enlarged storage lengthens recession timescales and thereby decreases the sensitivity of discharge to storage. In the recession period when recharge diminished, increased evaporation and decreased buffering effect of frost soils under warmer temperatures accelerate the initial recession of streamflow. By contrast, enlarged storage and lengthened recession timescales slow down the recession. While reservoir regulations in some basins have helped reduce and even reverse some of these climate warming effects, this short-term remedy could only function before the solid water storage is exhausted when the climate warming continues.

Keywords. Rising temperatures; Streamflow recession characteristics; Change of storage-discharge relationship; Permafrost degradation; Glacier melting

1. Introduction

The warming rates of air temperature in high latitudes and high altitudes are greater than the rate of change of global average near surface air temperature (e.g., Pepin et al., 2015). The greater climate warming has accelerated glacier melting and permafrost thawing in cold alpine regions, causing significant glacier and permafrost retreats (e.g., Yao et al., 2004, 2007) and landscape alternations (e.g., Niu et al., 2019). These changes undoubtably alter hydrodynamics of streamflow and groundwater storage in the alpine regions and their downstream tributaries (Bense et al., 2012; Walvoord and Striegl, 2007; Walvoord and Kurylyk, 2016; Li et al., 2018; Wang et al., 2018; Yi et al., 2021). A recent study of Wang et al. (2021) has shown that such changes have also caused changes of precipitation-streamflow relationship. The societal impacts of these changes are profound because they redefine freshwater availability and its seasonality for populations of billions in the downstream tributaries (e.g., Cuo et al., 2014; Zhang et al., 2013; Wang et al., 2020).

Many studies have found that compound effects of glacier and permafrost retreats in the past decades had reshaped the groundwater flow and hydrological cycle (e.g., Bring et al., 2016; Forster et al., 2014; Ji et al., 2020; Walvoord and Kurylyk, 2016). The accelerated glacier melting and permafrost thawing have increased the soil active layer thickness (ALT) and therefore enlarged groundwater storage and allowed exchange of the surface water and groundwater (Xu et al., 2017; Forster et al., 2014; Ji et al., 2020). Such exchange further alters streamflow composition in arctic catchments (Chang et al 2008; Walvoord and Kurylyk, 2016; Bring et al., 2016) and the northeastern and southern Tibetan Plateau (TP) (Li et al., 2018; Wang et al., 2018; Yi et al., 2021).

In those catchments, changes of groundwater storage and subsurface moisture profile due to permafrost retreat could reroute subsurface flow paths during low flows (Koch et al., 2014; Payn et al., 2012). The thickened ALT allows infiltration through the previously permafrost layer into aquifers and thus increases recharge in permafrost basins. It has been reported that the permafrost loss in the past decades has enhanced regional groundwater circulation (shortening its timescale) with more discharge to stream flows (Ji et al., 2020; Walvoord et al., 2012). As examples, the baseflow in the source region of the Yangtze River increased at a rate of 1.35 $mm \cdot a^{-1}$ during 1962–2012 following the annual temperature rise of 1.32℃ (Yi et al., 2021), and 1.09 $mm \cdot a^{-1}$ during 1979–2013 in glacierized basins in the TP with its annual temperature rise of 0.98℃ (Lin et al., 2020). Walvoord and Striegl (2007) found that the groundwater contribution to streamflow in an arctic basin increased by 0.7–0.9% per year from the 1950s to 2005 following its annual temperature rise of 1.24 ℃ during that period.

Effects of these changes of water budget and subsurface moisture profile on hydrograph are complicated in high altitude/frozen areas. The increase of ALT could reduce the buffering effect of soils on streamflow variability and thereby increase the baseflow recession rate (Lyon et al., 2009; Lyon and Destouni, 2010; Brutsaert and Hiyama, 2012). On the other hand, the increase of ALT enlarges groundwater storage and subsequently strengthens aquifer regulations on groundwater flow and slows the recession rate (Lin et al., 2020; Mao and Wang, 2016). These effects on recession rate can result in strong nonlinear behavior of streamflow in time and space.

During periods of little or no precipitation, the baseflow recession (dQ/dt vs. Q, where Q is discharge) is typically described by a power law $dQ/dt = -aQ^b$ (Brutsaert and Nieber, 1977; Tallaksen, 1995). The depletion of baseflow in relation to the parameters a and b contains valuable information concerning storage properties and aquifer characteristics of basins (Tallaksen, 1995). The recession scale parameter a is a function of the hydraulic and geometric properties of the aquifer of a basin and can be used as a proxy for effective depth to permafrost in frozen areas (Lyon and Destouni, 2010). The parameter b as reflected in the concavity of the hydrograph or the nonlinearity of recession (Dralle et al., 2017) is a function of boundary conditions to describe the equivalent water depth profile of an aquifer (Brutsaert and Nieber, 1977; Tashie et al., 2020). So, b can be interpreted as a measure of the diversity of water transport timescales throughout various parts of a catchment (Harman et al., 2009). Therefore, the variations of a and b in time and space can describe recession characteristics of a basin (e.g., Brutsaert and Nieber, 1977; Kirchner, 2009).

For the effects of a and b on the recession characteristics, Tashie et al. (2019) defined $\log(a)$ as the stability of streamflow, and b as recession nonlinearity. For individual events, an increase in the relative value of a between events indicates decreased streamflow stability, while an increase in b indicates increased nonlinearity. Changes of the recession characteristics in time reflect their vulnerability to climatic and anthropogenic forcings (Berghuijs et al., 2016; Brooks et al., 2015; Buttle, 2018). Streamflow stability, $\log(a)$, has a significant seasonal cycle in over 99% of basins in the Continental United States (Tashie et al., 2020). Moistening climate in catchments could increase the diversity of flow paths and the nonlinear relationships between storage/recharge and discharge (Brutsaert and Nieber, 1977; Hinzman et al., 2020). In cold climate regions, reduced glacier size can lead to considerable amplification of seasonality of streamflow (Juen et al., 2007; Vuille et al., 2008). Hinzman et al. (2020) reported a widespread increase in nonlinearity of recessions in Northern Sweden due to climate warming. In addition, they found that this nonlinearity is significantly higher in warm winters than in cold winters. These analyses were performed under the assumption that a and b are effectively decorrelated. However, because changes of a in time are dependent on discharge Q, $\log(a)$ may be strongly correlated with b in individual events (Dralle et al. 2015 and Biswal, 2021). Dralle et al. (2015) proposed a rescaling technique that eliminates the scale dependence of fitted power law parameters. Biswal (2021) selected the median of the values of b in individual events as the fixed b value and used it to find the event values of a.

In the southern TP, the Yarlung-Zangpo River basin (YRB, Fig. 1a) has decades of observations and offers an opportunity to estimate variations of recession characteristics of streamflow in glaciated areas of TP. Using those data, some recent studies have shown that the climate of the area has become warmer and wetter from 1980-2015 (e.g., Wang et al., 2021). Climate warming has reduced the buffering effect of glacial and permafrost on streamflow, leading to catchment property change with shorter streamflow response time to precipitation (Wang et al., 2021). These changes must have affected streamflow recession characteristics.

The objective of this study is to investigate temporal and spatial variations of streamflow recession characteristics driven by climate and landscape changes in the glaciated basin of YRB. The changes of these characteristics are examined using comparisons and contrasts of streamflow recessions in different sub-basins and time periods according to the power law. To

describe the temporal variability of the recession characteristics under climate warming, the decorrelation method by Dralle et al. (2015) is used to obtain a recession parameter a' independent of b from individual recessions over the period of 1980-2015. Then, the a' and b are regressed with mean temperature in recession periods for each sub-basin of YRB. Sensitivity analysis reveals the effect of climate warming on the recession parameters, recession rates, and storage/recharge-discharge relations of different sub-basins of YRB. They show the extent of the nonlinearity in the variation of the streamflow recessions in this glaciated basin of TP.

2. Study region and data

The YRB (28.2°–31.2°N, 82.0°–94.9°E) is the largest river basin in TP (Fig. 1). The main stem of YRB is formed by major suture zones in southern TP from the collision of the Indian plate and the Eurasian plate. The modern YRB flows along the suture from the west to the east before bending to the south at the eastern Himalayan syntaxes with an average west-east gradient about 2.63‰ (Fig. 1a) (Tan et al., 2021). In this study, we selected the upstream of Great Gorge of YRB (main stem about 1100 km with an area of 2.0 $\times 10^5$ km^2). The elevation of the study area drops drastically from 6234 m in the west to 2030 m in the east (You et al. 2007, Wang et al., 2021).

Climate in YRB is heavily influenced by the Indian monsoon in summer and the westerlies in winter (Ren et al., 2018; Tian et al., 2020). From the west to the east of the basin, mean annual temperature varies from -9.3° to 22.0°C, and the mean annual precipitation from 300 to 1050 mm. Nearly 90% of annual precipitation falls during June to September. As a result, the mean annual total streamflow of the entire basin, 289.7 mm, is highly unevenly distributed in seasons. The summer streamflow is derived from monsoon rainfall and glacier meltwater. Groundwater accounts for about 55% of the annual streamflow in upstream and 27% in downstream of YRB (Yao et al., 2021).

There are four hydrological stations along the main stem of YRB: LZ, NGS, YC, and NX shown in Fig. 1a. Two additional hydrological stations, YBJ and LS, are located in the major tributaries of the Lhasa River which originates from the Nyainqêntanglha Mountains north of YRB (Fig. 1a). Daily streamflow data from 1980 to 2015 are available at these hydrological stations, except LZ. Accordingly, we divide YRB into five sub-basins, with three nested sub-basins of NGS, YC, and NX in the main stem of YRB, and two sub-basins of YBJ and LS in the tributaries of the Lhasa River.

There are four main dams/reservoirs (marked by the purple squares in Fig. 1a) in YRB above the hydrological station of NX. The reservoirs, ML, ZK, PD, and ZM, were built in 1999, 2003, 2007, and 2014, respectively. The reservoir ML, PD, and ZM are operated daily while ZK is operated seasonally. The impact of reservoir regulations on streamflow is minor for the sub-basins NGS, YC, and NX in the main stem of YRB because the reservoirs are daily operated and affect less than 10% of the areas of the tributaries. In the tributary of the Lhasa River, the sub-basin YBJ has no reservoirs while the sub-basin LS has two reservoirs, PD and ZK, which have impacts on streamflow.

Daily gridded data (0.1°×0.1 °spatial resolution) of precipitation (P) and mean surface air temperature (T) during 1980–2015 were provided by the National Tibetan Plateau Data Center (Yang and He, 2019; He et al., 2020; http://data.tpdc.ac.cn). The sub-basin averaged P and T are calculated by the geometric mean of the gridded data.

Data of the glacier area and permafrost area, and the normalized difference vegetation index (NDVI) were collected from National Tibetan Plateau Data Center (Table 1, http://data.tpdc.ac.cn). Glacier areas are located at altitudes from 3370 to 6460 m above the sea level (Fig. 1a). Before 2000, the glacier and permafrost area account for 1.88% and 41.8% of the YRB area, respectively. These coverage percentages have reduced prominently since 2000 (Table 2). The annual mean NDVI was calculated by the maximum value synthesis method from the Global GIMMS NDVI3g v1 dataset with a 15-day temporal resolution and 1/12° spatial resolution. The vegetation types are mainly alpine meadow, alpine steppe in the upstream (LZ), alpine shrubs and grasslands in the middle region (LZ-NGS), and alpine grassland and forest in the lower YRB (NGS-NX) (Liu et al., 2014).

The annual depth of glacial melt data (G) during 1980–2015 is estimated using the degree-day model (Su et al., 2015; Liu and Zhang, 2018). The calculation procedures are detailed in Wang et al. (2021). The annual ALT is estimated using a linear statistical function of air freezing index (FI_{air}) described in Xu et al. (2017) where FI_{air} is calculated according to the cumulative value of daily mean temperature below 0℃ in a year.

After the warm season (June-September), there is little precipitation (Hayashi, 2020) in YRB and the melting of snow and glacier is minor due to cold temperatures (<-5 °C, Fig. 3). Subsequently, the flow discharge recedes from September to February of the following year. In this study, we use the daily discharge (Q_t) in this recession period, which is defined from 1 October to 15 February of the following year, in our analysis of the recession process.

3. Methodologies

3.1 Detection of changes in annual climate and hydrological series

The Mann-Kendall (MK) method (Mann, 1945; Kendall, 1975) combines trend-free pre-whitening treatment (TFPW-MK) (Yue and Wang, 2002) with Sen-slope (Sen 1968). The TFPW-MK is used in this study to test the temporal trend of annual variations of meteorological and hydrological elements at the specified significance level of α=0.05.

The Pettitt method is applied to detect the change point (year) of annual hydrological and meteorological variables. Pettitt method is nonparametric and has been widely used in mutation point detection (Pettitt, 1979; Mallakpour et al., 2016; Wang et al., 2021).

3.2 Streamflow recession analysis

Based on analytical solutions to the Boussinesq equation, the relationship of streamflow (Q in units of $mm \cdot d^{-1}$) and streamflow change ($-dQ/dt$, $mm \cdot d^{-2}$) in a recession period can be expressed by the power-law (Brutsaert and Nieber, 1977):

$$-dQ/dt = aQ^b \quad (1)$$

where a ($mm^{1-b} \cdot d^{b-2}$) and b (dimensionless) are the recession coefficients (Brutsaert and Nieber, 1977; Tashie et al., 2020). Based on (1), the relationship between groundwater storage (S) and streamflow can be derived

$$S = KQ^m \quad (2)$$

where $K = [a \cdot (2-b)]^{-1}$ ($mm^{b-1} \cdot d^{2-b}$) and $m=2-b$.

The recession timescale (τ) measures the recession rates of individual recessions (Kirchner, 2009) and is defined as

$$\tau = \frac{dS}{dQ} = \frac{1}{aQ^{b-1}} \quad (3)$$

From (1) – (3), the storage sensitivity of discharge (λ_S) for the recession curve (Berghuijs et al., 2016) is

$$\lambda_S = \frac{dQ/Q}{dS} = \frac{1}{\tau Q} = aQ^{b-2} \quad (4)$$

where λ_S (mm^{-1}) is a measure of the sensitivity of instantaneous discharge values to water storage changes, and indicates the fractional increase in discharge for each unit of increase in storage. The larger (or smaller) the values of a (or b) are the more sensitive is the discharge to water storage.

Both the relationships of $-dQ/dt \sim Q$ and $S \sim Q$ are linear if $b=1$ and nonlinear if $b \neq 1$. When $b \neq 1$, the discharge recession is

$$Q_t = Q_0(1 + Q_0^{b-1}a(b-1)t)^{1/(1-b)} \quad (5)$$

where Q_0 and Q_t are initial ($t = 0$) discharge and discharge at time t. For any specific initial discharge Q_0, the larger the b is the faster the hydrograph recession is for high discharge and the more stable the recession is for low discharge (Tashie et al., 2020).

The parameters a and b can be determined by fitting the daily observation data of $(\Delta Q/\Delta t) \sim Q$ in log–log diagram using linear least-squares regression. The fitted values of a and b are used to estimate $-dQ/dt$ and Q_t using (1) and (5). The accuracy of the estimated $-dQ/dt$ values is evaluated by the root-mean-square logarithmic error (RMSLE) (Bekele and Nicklow, 2007)

$$\text{RMSLE} = \left[\frac{1}{N}\sum_{i=1}^{N}(\log(-dQ_{est}(i)/dt) - \log(-dQ_{obs}(i)/dt))^2\right]^{1/2} \quad (6)$$

where $Q_{obs.i}$ and $Q_{est.i}$ are the observed and estimated discharges, respectively. The terms $dQ_{est}(i)/dt$ and $dQ_{obs}(i)/dt$ in (6) are derived from taking derivatives of (1). In practice, their finite difference $\Delta Q/\Delta t$ is determined from the observed recession segments ΔQ in time interval Δt. N in (6) is the number of data points of $-dQ/dt$ in individual recessions.

According to Dralle et al. (2017), by minimizing

$$E_{MAP} = \frac{1}{N}\sum_{i=1}^{N}\left|\frac{Q_{obs,i} - Q_{est,i}}{Q_{obs,i}}\right| \quad (7)$$

where E_{MAP} is the absolute relative error between $Q_{obs.i}$ and $Q_{est.i}$ over the recession period, a fitting in each recession hydrograph would ensure that the estimated volume of recession discharge approaches to that of the observed recession.

To avoid recession parameter scale dependence, we use the method of Dralle et al. (2015) and rescale the discharge Q by $Q = k\hat{Q}$. The revised power law for the rescaled discharge $\hat{Q}$ is

$$\frac{d\hat{Q}}{dt} = -ak^{b-1}\hat{Q}^b = -a'\hat{Q}^b \quad (8)$$

where k is a constant and $a' = ak^{b-1}$ is a new recession parameter independent of b. The unit of a' is d^{-1} (Dralle et al., 2015). Furthermore, to minimize the correlation of the fitted recession exponent and log-transformed fitted recession scale parameters for a unique value of k, we use the following equation to compute the scaling factor k according to Bergner and Zouhar (2000)

$$k = \exp\left(-\frac{\sum_{i=1}^{n}(b_i-\bar{b})(log(a_i)-\overline{\log(a)})}{\sum_{i=1}^{n}(b_i-\bar{b})^2}\right) \quad (9)$$

In (9), $\bar{b}$ and $\overline{\log(a)}$ are the arithmetic mean of annually fitted recession exponents $\{b_1, b_2, \dots, b_n\}$ and log-transformed fitted recession intercepts $\{\log(a_1), \log(a_2), \dots, \log(a_n)\}$, respectively, and i is the number of annual values from 1980 to 2015.

3.3 Changes of recession characteristics under warming climate

In cold climate regions, recession coefficients are closely related to the thickness of the active layer in soil profile above permafrost layer (Bense et al., 2012; Brutsaert and Hiyama, 2012). Changes of these catchment properties depend on daily, seasonal, and annual temperature variability. For example, the transition from unfrozen to frozen ground for temperature varying between 0 and -0.5°C coincides with a reduction in hydraulic conductivity of several orders of magnitude for saturated porous media (Burt and Williams, 1976). On the other hand, when temperature rises, the thawing front in the active soil layer moves progressively downward as summer proceeds, leading to increasing water storage in the active layer. If the frozen soil beneath the thawing front is ice-saturated (thus relatively impermeable), the active soil layer can function as a very shallow perched aquifer that controls streamflow response to snowmelt and summer precipitation (Carey and Woo, 2005; Yamazaki et al., 2006; Wright et al., 2009; Koch et al., 2014). To include these variations in a study, recession coefficients are considered varying dependent on watershed state and temperatures (Tashie et al., 2019).

In this study, the variability of the parameters a' and b are expressed as a function of temperature (T), i.e., $a'(T)$ and $b(T)$ as follows

$$\begin{cases} a'(T) = \alpha \cdot \exp(\alpha_1 T) \\ b(T) = \beta \cdot \exp(\beta_1 T) \end{cases} \quad (10)$$

where α and α_1 are coefficients for $a'(T)$, β and β_1 are coefficients for $b(T)$, and T is the mean surface air temperature in the recession period (T_{re}). These coefficients can be obtained by fitting the recession parameters of individual recession events with known T_{re} in each sub-basin.

From (2), the temporal change of S (ΔS) can be described

$$\Delta S = \frac{\partial S}{\partial K}\Delta K + \frac{\partial S}{\partial m}\Delta m + \frac{\partial S}{\partial Q}\Delta Q \quad (11)$$

Incorporating $K = k^{b-1}/[a'\cdot(2-b)]$ and $m = 2-b$, we can write ΔS as

$$\Delta S = \frac{\partial S}{\partial K}\frac{\partial K}{\partial a'}\Delta a' + \left(\frac{\partial S}{\partial K}\frac{\partial K}{\partial b} + \frac{\partial S}{\partial m}\frac{\partial m}{\partial b}\right)\Delta b + \frac{\partial S}{\partial Q}\Delta Q \quad (12)$$

or

$$\Delta S = \lambda_{a'}\Delta a' + \lambda_b \Delta b + \lambda_Q \Delta Q \quad (13)$$

where $\lambda_{a'}$, λ_b, and λ_Q are the sensitivity coefficients of ΔS to a', b, and Q, respectively, and can be derived as follows

$$\begin{cases} \lambda_{a'} = \frac{\partial S}{\partial K}\frac{\partial K}{\partial a'} = \frac{-k^{b-1}}{a'^2(2-b)}Q^{2-b} \\ \lambda_b = \frac{\partial S}{\partial K}\frac{\partial K}{\partial b} + \frac{\partial S}{\partial m}\frac{\partial m}{\partial b} = \frac{k^{b-1}}{a'(2-b)}Q^{2-b}\left(\frac{1}{2-b} - \ln Q\right) \\ \lambda_Q = \frac{\partial S}{\partial Q} = \frac{k^{b-1}}{a'Q^{b-1}} = \tau \end{cases} \quad (14)$$

Because the recession parameters a' and b are functions of T in (8) S is a function of T and Q. The change of S (ΔS) can therefore be expressed as

$$\Delta S(T) = \frac{\partial S}{\partial T}\Delta T + \frac{\partial S}{\partial Q}\Delta Q \quad (15)$$

or

$$\Delta S(T) = \lambda_T \Delta T + \lambda_Q \Delta Q \quad (16)$$

where λ_T is the sensitivity coefficient of ΔS to T. λ_T can be derived as

$$\lambda_T = \frac{\partial S}{\partial T} = \frac{k^{b-1}}{a'(2-b)}Q^{2-b}\left(\frac{b(\beta_1+\alpha_1)-2\alpha_1}{2-b} - b\beta_1 \ln Q\right) \quad (17)$$

4. Results

4.1 Spatial and temporal variations of climate and hydrological variables

4.1.1 Spatial variations

The mean values of the observed climate and hydrological variables during 1980–2015 in the sub-basins have shown that the region's climate has become warmer and wetter (Fig. 2a–2c and Table 2). The wet trend is largest in YBJ and LS sub-basins. We note that the mean temperature of YBJ is lowest among the sub-basins because most of its area is at higher altitudes. It has the largest fractional glacier coverage area about 10%. The percentage of glacier area in the other sub-basins is 1.63%,

1.52%, 1.92% and 0.75% in NGS, YC, NX, and LS sub-basin, respectively. The percentage of permafrost area (PPA) ranges from 41.8%–47.7% in the five sub-basins.

The mean annual streamflow (Q) and streamflow in the recession period (Q_{re}) (both in units of mm) increased (Figs. 2d and 2e), resulting in higher runoff coefficient Rc (R/P) towards the wetter downstream of the main stem of YRB. However, the wettest sub-basins of YBJ and LS do not have the greatest discharge and high Rc, possibly because of the icy environment. Daily coefficient of variation (CV) of streamflow is higher in YBJ and LS and in upstream of NGS. CV decreases towards the wetter downstream of YRB, partially because of strengthening watershed regulation as the sub-basin areas increase and the dams are included in the area of the analysis.

4.1.2 Annual variations of climate and hydrological variables during 1980–2015

Figures 2a–2f show variations of the observed climate and hydrological variables from 1980 to 2015. Tested by TFPW-MK, annual mean temperature (T) and temperature in the recession period (T_{re}) rose significantly ($p < 0.05$) in all sub-basins of YRB (Figs. 2a and 2b). Annual T rose at a rate of 0.045°–0.075°C·a^{-1} for the five sub-basins, smaller than the rate of 0.070°–0.097°C·a^{-1} for annual T_{re}. Annual precipitation (P) also increased, tested to be significant ($p < 0.1$), in the sub-basins of YC, NX, and LS, but insignificant in NGS and YBJ (Fig. 2c). Annual glacier meltwater G and the total number of days with mean temperature above 0°C in a year (MTD_a) increased significantly in all sub-basins (Figs. 2f and 2j). Meanwhile, the total number of days with mean temperature above 0°C in the recession period (MTD_{re}) also increased, and it was tested to be significant in the mainstream of YRB (e.g., NGS, YC, and NX), and insignificant in the two sub-basins of YBJ and LS (Fig. 2k). The rate of G increase is from 0.46 mm·a^{-1} in LS to 2.86 mm·a^{-1} in YBJ. The rate of increase of annual MTD_a and MTD_{re} is 0.48–0.82 d·a^{-1} and 0.12-0.32 d·a^{-1}, respectively, in the five sub-basins. Under the warmer and wetter climate, vegetation coverage trended to increase. NDVI increased at a rate of 5.1^{-4}–8.03^{-4} a^{-1} during 1980–2015 in the four sub-basins YC, NX, NGS, and YBJ, but decreased at a rate of -1.03^{-4} a^{-1} in LS (Fig. 2g).

Over the same period, the annual mean discharge Q and the mean discharge in the recession period Q_{re} increased significantly, except for Q_{re} in LS sub-basin (Figs. 2d and 2e). The Q increased at a rate of 1.16–1.68 mm·a^{-1}, higher than the rate of 0.22–0.47 mm·a^{-1} for Q_{re}. In contrast, Q_{re} in LS decreased insignificantly (Fig. 2d), possibly because of initial water storage when the ZK reservoir (Fig. 1a) began operation around 2007.

In Wang et al. (2021), a point of dramatic change was detected around 1997 by the Pettitt' test for T, G, and Q, and around 1995 for annual P in the sub-basins of NGS, YC, and NX. In this study, the same point of change in 1997 was detected in the annual series of T_{re} and Q_{re} in NGS, YC, and NX sub-basins, and in the annual series of T, G, and Q in YBJ and LS sub-basins. The annual time series of Q in LS was detected to have two additional points of change in 1995 and 2005, possibly attributable to the increased impact of human (reservoir operation) activities (Cai et al., 2021). The point of change in 1997 has also been identified by the dramatic changes of surface conditions, i.e., the reversed NDVI trend (Fig. 2g), increased ALT (Fig. 2h), and accelerated thawing of permafrost after 1997 (Fig. 2i). Accordingly, we separate the study years from 1980–2015 into two periods: the early period from 1980 to 1996, and the recent period from 1997 to 2015.

Climate in the recent period has changed to be markedly warmer and wetter. The mean annual P after 1997 increased by 27–46 mm or 7.9–10.7% compared to that in the early period in the five sub-basins. The mean annual T in the recent period is 0.75°–1.52°C warmer than that in the early period, and a larger rise of 1.40°–1.78°C was found for the mean T_{re} after 1997. These changes concurred with 8.6–55.9 mm or 23.8–81.1% increase of mean annual G after 1997 in the five sub-basins. The mean MTD_a and MTD_{re} in the recent period is 8–18 days and 2–7 days greater than that in the early period of 1980–1996, respectively. As a result, Q increased by 29.6–50.2 mm or 12.7–31.5% in the recent period compared to that before 1997. This increase in Q as well as Q_{re} after 1997 is much larger in the upstream sub-basins NGS and YC.

4.1.3 Annual recession characteristics

As shown in Fig. 3, the annual hydrographs in the five sub-basins are consistent, delineating a single peak response to maximum precipitation as well as temperature in July–August. The statistic values of daily discharge series in the two periods show that the mean value in the recent period exceeds that in the early period in all sub-basins. Meanwhile, daily discharge variability in the recession of the annual hydrograph in the recent period is also greater than that of the early period, shown by larger CV after 1997 for most sub-basins, except sub-basin YBJ (Table 2).

Figure 4 further exhibits changes of recession rates are different in the early phase and the later phase of the recession for the selected hydrographs with approximately the same initial discharge Q_0 in each sub-basin. In the recent period, the streamflow recedes faster in the early phase of the recession and slows down in the later phase except LS.

The faster recessions in the recent periods are also illustrated by the regression on data points of $-dQ/dt$ vs. Q in log-log diagram (Fig. 5). The fitted line of $-dQ/dt$ vs. Q after 1997 has a steeper slope (Figs. 5a-5e) and a more negative intercept, except LS, indicating a higher value of b and a smaller value of a for the sub-basins of NGS, YC, NX, and YBJ after 1997. The increased b value and decreased a after 1997 suggest that the recession curves tend to be more concave for these sub-basins when the climate is warmer and wetter as indicated in Fig. 4. According to the non-overlapping moving averages of the 5-day series of the recession discharge, the estimated average recession rate after 1997 $[(\Delta Q/\Delta t)_2]$ is larger than that before 1997 $[(\Delta Q/\Delta t)_1]$ as indicated by the positive values of $\Delta v_Q = (\Delta Q/\Delta t)_2 - (\Delta Q/\Delta t)_1$ in Fig. 5f.

4.2 Estimation of the recession parameters

We used the observed hydrograph in each year and obtained the recession parameters a and b. Afterwards, a' is calculated using the scaling factor k (0.527, 0.602, 0.740, 0.594, and 0.611 $mm \cdot d^{-1}$ for NGS, YC, NX, YBJ, and LS, respectively). The results are summarized in Table 3. The mean values of annual a and a' during 1980–2015 range from 0.022 to 0.042 $mm^{1-b}\ d^{b-2}$ and from 0.015 to 0.025 d^{-1}, respectively, and the mean annual value of b ranges from 1.36 to 1.85 for the five sub-basins. Figure 6 shows the errors of the estimated recession (RMLSE and E_{MAP}) for the recession curve of each sub-basin. Mean annual RMLSE is less than 0.15 in all sub-basins. The mean annual E_{MAP} is lower than 10%, except in the sub-basins YBJ and LS where E_{MAP} is 0.15 and 0.14, respectively.

Figure 7 shows the relationship of annual value and 4–year moving average value of the recession parameters a' and b with mean surface air temperature in the recession period (T_{re}) in each sub-basin. The exponential function between a' or b and T_{re} is fitted with a high determination coefficient (R^2 ranges 0.51–0.67 for a' and 0.58–0.87 for b). These results show that a' decreases exponentially with increasing T_{re} in the sub-basins, except LS, while b increases exponentially with increasing T_{re} in all sub-basins.

For the multiyear mean values of parameters a, a' and b in the two periods (Table 3), the mean value of a and a' in the recent period ranges between 0.021–0.039 mm^{1-b} d^{b-2} and 0.014–0.023 d^{-1}, respectively, smaller than that in the early period when they range between 0.022–0.046 mm^{1-b} d^{b-2} and 0.015–0.027 d^{-1}, respectively, in the sub-basins, except LS. On the other hand, b ranges between 1.47–1.89 in the recent period, larger than that in the early period (1.25–1.81) for all sub-basins. These results indicate that warming and wetting climate increases the nonlinearity of the recession (b) and enhances stability of low streamflow [log(a)] for most sub-basins in YRB.

4.3 Change of storage-discharge relationship in warming climate

The strong sensitivity of the recession parameters of a (a') and b to T means that a warming climate can change the nonlinear relationship of the water storage (S) and discharge/streamflow (Q) (Eq. (2)). This change is shown by the increase of the recession coefficient K in the recent period (11.5–73.2 $mm^{b-1}\cdot d^{2-b}$ for ΔK in Table 3) and decrease of m (=2-b) in Eq. (2) because b increases with the temperature (Table 3 and Fig. 7). The increase of K and decrease of m mean a lower discharge for a specific storage or a higher storage for a specific discharge in the recent warmer period. As an example, we show in Fig. 8 the relationship of S with Q for different K and/or m between the two periods in sub-basin YC. Q decreases significantly with the increase of K or decrease of m for storage S (Figs. 8a and 8b). The combination of the increase of K and decrease of m leads to marked decrease of Q for storage S (Fig. 8c). Correspondingly, the recession timescale (τ=dS/dQ) increases by 5.2–20.7 days in the recent warmer period in all sub-basins (Table 3), especially the glaciated sub-basin YBJ. The increase of τ also means increase in storage for Q because $S(Q)-S_0=\int_{S_0}^{S} dS=-\int_{Q_0}^{Q}\tau(Q)dQ>0$ in the recession.

The lower discharge for a specific storage or higher storage for any specific discharge are further shown by the results of the storage sensitivity of discharge (λ_S in Eq. (4)) in Table 4. The mean value of λ_S during 1980–2015 ranges between 0.036 and 0.059 mm^{-1} for the five sub-basins. These values mean that 1 mm decrease in storage only results in 3.6–5.9% decrease in discharge. Thus, in a warmer climate a unit decrease in storage releases less water to discharge in the recession period, supported by the decrease of λ_S in the recent warmer period (see the negative values of $\Delta\lambda_S$ in Table 4), and towards the warmer and wetter downstream for the main stem of YRB (from NGS to NX, see the mean annual value of λ_S during 1980–2015 in Table 4). This is especially so in glaciated basins, e.g., YBJ, where the decrease of λ_S ($\Delta\lambda_S$ in Table 4) is largest in the recent period, corresponding to the largest increase of τ. We also note that the decrease of λ_S ($\Delta\lambda_S$) in LS is relatively small in the recent period primarily because of regulation of reservoirs on discharge.

4.4 Sensitivity of recession parameters to storage change under climate warming

The change of sensitivity of discharge to storage (λ_S) should affect the recession processes. This effect is described by the sensitivity of the recession parameters to storage change ΔS ($\lambda_{a'}$ and λ_b for a' and b, respectively). As listed in Table 4, λ_b is positive while $\lambda_{a'}$ is negative in all five sub-basins. The larger negative $\lambda_{a'}$ is and the larger positive λ_b would be in the recent warmer period, particularly in the glaciated sub-basin YBJ ($\Delta\lambda_{a'}$ and $\Delta\lambda_b$ in Table 4). Thus, the increase of storage in warmer climate will correspondingly enhance the nonlinearity of recession (b) and streamflow stability [log(a)] in YRB, as indicated in Eq. (13). This sensitivity can be weakened however by anthropogenic effect (reservoir regulations) as suggested by the less sensitive result of the recession parameters of a' and b to ΔS in LS sub-basin.

Effects of climate warming on the change of the storage and streamflow recession characteristics can be further shown by storage change ΔS in response to changes of T and Q (ΔT and ΔQ) using Eq. (16). The values of λ_T in Table 4 show an increase in the recent period in all sub-basins, especially in YBJ and YC. Thus, the enlarged storage is largely attributed to climate warming. As expected, λ_T is smaller in the sub-basin LS with reservoir regulation. The values of λ_Q in Table 4 also become bigger in the recent warmer period in all sub-basins. These changes indicate that the climate warming increases storage and discharge.

However, the increase of discharge ΔQ in response to the increase in storage ΔS can be quite different in response to different rate of change of temperature ΔT in the five sub-basins. According to Eq. (16), the relationship between ΔS and ΔQ for different ΔT in the five sub-basins is shown in Fig. 9. As temperature rises, ΔS becomes greater while the greater increase of storage volume (in thawing soil layers) allows smaller amount of water to be released as baseflow. For example, as the mean annual temperature rises by 1.2℃ (ΔT = 1.2℃) the increase of discharge (ΔQ = 0.2 mm d^{-1}) corresponds to a storage increase of about 92 mm in NGS, 160 mm in YC, 63 mm in NX, 42 mm in LS, and a huge increase of 478 mm in YBJ (see the value of the ΔS vs. ΔQ in Fig. 9). These results suggest that a larger increase of water storage caused a smaller increase of baseflow in the glaciated sub-basins, reflecting a buffering effect of freezing on streamflow dynamics.

When the T_{re} increased from the early to the recent period, from -7.17 to -5.39 ℃ in NGS, -6.84 to -5.16 ℃ in YC, -6.54 to -5.02 ℃ in NX, -9.20 to -7.69 ℃ in YBJ, and -7.60 to -6.20 ℃ in LS, the estimated water storage in terms of $\lambda_T\Delta T$ in Eq. (16) increased between 15.2–132.6 mm for the five sub-basins. These increases contribute to about 86.4–99.9% of the total increase in storage ($\lambda_T\Delta T/\Delta S$) in those sub-basins. They only cause 0.1–13.6% increase of discharge in terms of $\lambda_Q\Delta Q/\Delta S$ in Eq. (16). This relationship varies among the five sub-basins with different glaciate conditions. In the warm and wet sub-basin NX with low glacial coverage, the increase in storage ($\lambda_T\Delta T$) is relatively small (35.4 mm and 86.4% of the total increase in storage) and the increase in discharge ($\lambda_Q\Delta Q$) is relatively large (5.56 mm and 13.6% of the total increase in storage). In the cold sub-basins with high glacial coverage, climate warming causes large increase of storage but small increase of discharge. As an example, the YBJ sub-basin has 97.3% of the total increase in storage vs. only 2.7% of the total increase in discharge. Again, this relationship is distorted in basins with human regulatory actions in water management. In the sub-basin LS with strong reservoir regulations, changes in both the storage and discharge are small (e.g., 0.1% in the total increase of storage).

5. Discussions

Observations have shown that climate warming has accelerated glacier melting and permafrost thawing in cold climate and high-altitude regions. Subsequent changes are found in vegetation growth and thickening of talik and active soil layer thickness. These changes have altered land surface conditions, unconsolidated soil profiles and subsurface permafrost, and thereby redefined surface and groundwater exchange and balance in those regions (Fig. 10). Our case study of YRB in southern TP shows that accelerated glacier melting and permafrost thawing during 1980–2015 have substantially increased its dynamic groundwater storage, defined as $S(Q) - S_0 = -\int_{Q_0}^{Q} \tau(Q) dQ$. These results with the decrease of terrestrial water storage (TWS) in south TP, including YRB (Wang et al., 2020) in recent decades, indicate that a transform of water storage in the region from solid form (glacier and permafrost) to liquid volume (soil moisture, surface water in rivers/lakes, and groundwater) (Fig. 10b). According to water balance in a catchment, i.e., $dS/dt = P_r - E - Q$ where S is regarded as the "liquid volume" (here, change of S is equal to the sum of changes in soil moisture and groundwater), E is evapotranspiration, and P_r is the recharge from glacier melting, permafrost thawing and precipitation, the increase of S infers that P_r is larger than the sum of E and Q in a study region. Because cold regions tend to have a greater coverage percentage of glacier and permafrost, glacier melting and permafrost thawing could substantially increase water storage under climate warming. Higher water storage could extend the recession period and sustain healthy annual streamflow.

Our study also shows that the increase of water storage and its effect on the annual recession of streamflow weakened towards the warmer downstream areas of YRB (with diminishing glacier melting and permafrost thawing effect). Accordingly, if the climate warming continues, the shrinking of glacier and permafrost volume could eventually reach a point when there is not enough melting to recharge the liquid volume of water in YRB. From that point onward, steady streamflow in YRB would be in danger.

While the processes initiated by the accelerated glacier melting and permafrost thawing extend subsurface flow paths (Hinzman et al., 2020) and the streamflow recession time (τ), the increase of surface temperature and E can also increase surface water loss. According to the discharge relation $-dQ/dt = -\frac{dQ}{dS}\frac{dS}{dt} = (-P_r + E + Q)/\tau$ (Kirchner, 2009), where P_r can be neglected in the recession period, a faster recession ($-dQ/dt$) could occur under climate warming from faster decrease of storage (dS/dt) due to increasing of E (Tashie et al., 2020) as well as faster response of discharge to storage (dQ/dS) due to the increase of the effective hydraulic properties (Lamontagne-Hallé et al., 2018). This phenomenon has happened for the initial recession period of 1-2 months when temperature is relatively higher (see Fig. 4).

Meanwhile, the accelerated glacier melting and permafrost thawing have shortened the frost period (i.e., the prolonged MTD_a and MTD_{re} in Figs. 2j and 2k), and thereby increased the soil active layer thickness (ALT) for groundwater storage (Lamontagne-Hallé et al., 2018), lengthened subsurface flow paths (Hinzman et al., 2020), and the streamflow recession time (τ). These changes weaken the sensitivity of discharge to the storage ($dQ/dS = 1/\tau$) and slow down the recession rate ($-dQ/dt$), found in the later recession period when temperature is relatively lower (see Fig. 4). Therefore, the competing effects from the warming climate on dS/dt and dQ/dS in different recession phases would lead to the recession curve becoming more concave,

which indicates an increase of the nonlinearity of the recession (b) and streamflow stability [log(a)] in YRB. In comparison, in the warm climate area, the effect of storage decrease (dS/dt) on recession (-dQ/dt) strengthens, and the effect of the recession timescale ($1/\tau$ or dQ/dS) on the recession weakens. As shown in Fig. 9, when temperature is higher (e.g., large and positive ΔT), hydrograph recession (negative ΔQ) is faster along with the faster decline of storage (ΔS).

Additionally, deep circulating groundwater through macro structures, such as north–south oriented active tensile faults (Fig. 1b) could also affect baseflow and its recharge and discharge (Tan et al., 2021). According to studies using multi-tracer data (e.g., ^{2}H, ^{3}H, ^{18}O, and Sr), modern meltwater is found to primarily maintain the rapid recharge of phreatic groundwater in alpine regions through faults and fissures (Shi et al., 2021). In the middle of YRB (i.e., NGS-YC sub-basins), changes of storage sensitivity to temperature (λ_T in Table 4) and recession timescale (τ) are greater than those in the upstream and downstream areas (NGS and NX sub-basin, respectively). Rising temperature can greatly increase storage (Fig. 10b).

Finally, the anthropogenic effects from reservoir regulation can reduce the climate warming effect on these storage-discharge responses in YRB. For example, in the LS sub-basin, operations of two reservoirs significantly reduced the sensitivity of the recession parameters a (a') and b to climate warming, and increased streamflow stability [log(a)] (Fig. 4e). It remains questionable however as how this human effort in water management in YRB would be practical/beneficial after the point when the increase of water storage from glacier and permafrost melt has exhausted the solid volume of water resources in the basin following the climate warming.

6. Concluding remarks

Climate warming accelerated after 1997 in the Tibetan Plateau, especially in its cold and high-altitude upstream areas. Since 1997, the mean annual temperature has risen by 0.75°–1.52°C, and the mean temperature in the annual recession period (1 October – 15 February of the following year) has risen by 1.40°–1.78°C in the five sub-basins of YRB. The largest rise of temperature occurred in the drier and colder sub-basins in the upstream YRB. The recent strong warming has accelerated glacier melting and permafrost thawing, and thereby increased annual streamflow (12.7–31.5% larger than the mean value in the early period before 1997) and streamflow in the recession period (20.9–25.8% larger than before 1997) for the five sub-basins, except LS where reservoir operations are active and heavily affecting the streamflow. These processes initiated by climate warming have changed the hydrological properties of sub-basins considerably and altered the recession characteristics and the storage-discharge relationships.

We have found that the recession parameter a (a') that characterizes the stability of streamflow has decreased exponentially in the sub-basins, except LS. Meanwhile, the parameter b that describes the nonlinearity of the recession to discharge has increased exponentially in all the sub-basins. These results indicate that climate warming increases the nonlinearity of the recessions and enhances streamflow stability in most of the sub-basins in YRB. Our sensitivity analysis further shows the decrease of the sensitivity of discharge/streamflow to storage under the warming climate. Currently, the accelerated glacier melting and permafrost thawing have recharged the system, deepening the active subsurface zone and

increasing groundwater storage. Only a small fraction of the enlarged storage is released in surface streams because the increase of active water layer lengthens subsurface flow paths. These changes have also increased the recession timescale and retarded the recession in the later period, particularly in high altitude cold climate areas. In the relatively warm climate areas downstream of YRB, the effect of these changes is minor.

As the liquid water storage has increased greatly from melting glaciers and thawing permafrost in YRB in the recent warming climate, the fast erosion of the solid water storage has weakened its buffering effect of the streamflow which is becoming less stable and more vulnerable to individual intense precipitation events, such as increase of the recession rate in the initial period found in this study. There are two potential consequences from these changes: one is the increase of flush flooding in the trend of rising precipitation in the high-altitude sub-basins where more land is exposed after the retreat of glaciers, and the other is the extreme scenario of exhaustion of the water resources in the upstream of YRB after the buffering effect of glacier and permafrost is lost following the continued warming of the climate.

While human interference with these processes, via reservoirs and regulations, can reduce and curb these impacts of climate warming on storage-discharge relationships, recession characteristics, and streamflow in short term, as shown in the sub-basin LS, long-term strategies need to be developed to not only cope with the short-term needs but also the sustainability of water resources in the Tibetan Plateau under the threat of the continued warming that could change the entire hydrological system in this critical source region of water for the world most populated nations.

Code and data availability

All codes and results developed in this work and presented/discussed in this paper are available upon request to the corresponding author. The sources of data used in this paper are listed in Table 1 and are accessible at their websites.

Author contributions

Jiarong Wang: Writing-original draft, Investigation, Methodology, Data curation, Visualization. Xi Chen: Conceptualization, Writing-review & editing, Formal analysis, Funding acquisition. Man Gao: Methodology, Data curation. Qi Hu: Writing-review & editing. Jintao Liu: Data curation, Validation.

Competing interest

The authors declare that they have no conflict of interest.

Acknowledgments

We thank Dr. Rupp and two anonymous reviewers for their valuable comments that have led to improvements of the contents and clarity of this manuscript. The work presented in this paper has been supported by the National Natural Science Foundation of China (NSFC) (No. 91747203; 41901029) and the Second Tibetan Plateau Scientific Expedition and Research Program (STEP; Ministry of Science and Technology, MOST; No. 2019QZKK0207). Qi Hu's contribution was supported by USDA Cooperative Research Project NEB-38-088.

References

Bekele, E.G., Nicklow, J.W.: Multi-objective automatic calibration of SWAT using NSGA-II, Journal of Hydrology, 341 (3), 165–176, doi: 10.1016/j.jhydrol.2007.05.014, 2007.

Bense, V.F., H. Kooi, G. Ferguson, and T. Read.: Permafrost degradation as a control on hydrogeological regime shifts in a warming climate, Journal of Geophysical Research: Earth Surface, 117. doi:10.1029/2011JF002143, 2012.

Berghuijs, W. R., Hartmann, A., & Woods, R. A.: Streamflow sensitivity to water storage changes across Europe, Geophysical Research Letters', 43, 1980–1987, doi: 10.1002/2016GL067927, 2016.

Bergner, F., and G. Zouhar.: A new approach to the correlation between the coefficient and the exponent in the power law equation of fatigue crack growth, International journal of Fatigue, 22(3), 229–230, doi:10.1016/S0142-1123(99)00123-1, 2000.

Biswal, B.: Decorrelation is not dissociation: there is no means to entirely decouple the Brutsaert-Nieber parameters in streamflow recession analysis, Advances in Water Resources, 147, 103822, doi:10.1016/j.advwatres.2020.103822, 2021.

Bring, A., Fedorova, I., Dibike, Y. B., Hinzman, L. D., Mard, J., Mernild, S. H., Woo, M.: Arctic terrestrial hydrology: A synthesis of processes, regional effects, and research challenges, Journal of Geophysical Research G: Biogeosciences, 121, 621–649. doi:10.1002/2015JG003131, 2016.

Brooks, P., Chorover, J., Fan, Y., Godsey, S. E., Maxwell, R. M., McNamara, J., and Tague, C.: Hydrological partitioning in the critical zone: Recent advances and opportunities for developing transferable understanding of water cycle dynamics, Water Resources Research, 51, 6973–6987, doi:10.1002/2015WR017039, 2015.

Brutsaert, W. and Nieber, J. L.: Regionalized drought flow hydrographs from a mature glaciated plateau, Water Resources Research, 13, 637–643, doi:10.1029/WR013i003p00637, 1977.

Brutsaert, W., and T. Hiyama.: The determination of permafrost thawing trends from long-term streamflow measurements with an application in eastern Siberia, Journal of Geophysical Research: Atmospheres 117(D22). doi:10.1029/2012JD018344, 2012.

Burt, T.P., and P.J. Williams.: Hydraulic conductivity in frozen soils, Earth Surface Processes, 9(4):411–416. doi: 10.1002/esp.3290010404, 1976.

Buttle, J. M.: Mediating stream baseflow response to climate change: The role of basin storage, Hydrological Processes, 32, 363–378, doi: 10.1002/hyp.11418, 2018.

Cai Lichen, Li Zhiwei, You Yuchi, & Huang Cai.: Analysis of runoff changes in Lhasa River from 1956 to 2016 and the influencing factors, Journal of Water Resources and Water Engineering, 32(02), 90-96, (in Chinese) 2021.

Carey, S.K., and M. K. Woo.: Freezing of subarctic hillslopes, Wolf Creek Basin, Yukon, Canada, Arctic, Antarctic, and Alpine Research, 37:1–10, doi: 10.1657/1523-0430(2005)037[0001: FOSHWC]2.0.CO;2, 2005.

Chang X, Jin H, He R, Yang S, Yu S, Lv L, Guo D, Wang S and Kang X.: Advances in permafrost and cold regions environments studies in the Da Xing'anling (Da Hinggan) mountains, northeastern China, Journal of Glaciology and Geocryology, 30 176–82, doi: 10.1007/s11442-008-0201-7, (in Chinese) 2008.

Cheng, G., Jin, H.: Permafrost and groundwater on the Qinghai-Tibet Plateau and in northeast China, Hydrogeology Journal, 21, 5–23. doi: 10.1007/s10040-012-0927-2, 2013.

Cuo, L., Zhang, Y. X., Zhu, F. X., and Liang, L. Q.: Characteristics and changes of streamflow on the Tibetan Plateau: A review, Journal of Hydrology, 2, 49–68, doi: 10.1016/j.ejrh.2014.08.004, 2014.

Dralle, D. N., Karst, N. J., Charalampous, K., Veenstra, A., & Thompson, S. E.: Event-scale power law recession analysis: Quantifying methodological uncertainty, Hydrology and Earth System Sciences, 21(1), 65–81, doi: 10.5194/hess-21-65-2017, 2017.

Dralle, D., Karst, N., Thompson, S. E.: a, b careful: The challenge of scale invariance for comparative analyses in power law models of the streamflow recession, Geophysical Research Letters, 42(21), 9285-9293, doi: 10.1002/2015GL066007, 2015.

Forster, R. R., Box, J. E., Van Den Broeke, M. R., Miège, C., Burgess, E. W., Van Angelen, J. H., et al.: Extensive liquid meltwater storage in firn within the Greenland ice sheet, Nature Geoscience, 7(2), 95– 98. doi: 10.1038/ngeo2043, 2014.

Ge S, McKenzie J, Voss C and Wu Q.: Exchange of groundwater and surface-water mediated by permafrost response to seasonal and long term air temperature variation, Geophysical Research Letters': 38 L14402, doi: 10.1029/2011GL047911, 2011.

Harman, C. J., Sivapalan, M., & Kumar, P.: Power law catchment-scale recessions arising from heterogeneous linear small-scale dynamics, Water Resources Research, 45, W12601, doi: 10.1029/2008WR007392, 2009.

Hayashi, M.: Alpine Hydrogeology: The Critical Role of Groundwater in Sourcing the Headwaters of the World, Groundwater, 58(4), 498– 510, doi: 10.1111/gwat.12965, 2020.

He, J., Yang, K., Tang, W., Lu, H., Qin, J., Chen, Y., & Li, X.: The first high-resolution meteorological forcing dataset for land process studies over China. Scientific Data, 7, 25, doi: 10.1038/s41597-020-0369-y, 2020.

Hinzman, A.M., Lyon, S.W., Ploum, S.W., Sjoberg, Y., van der Velde, Y.: Increasing non-linearity of the storage-discharge relationship in sub-Arctic catchments, Hydrological Processes, 34 (19), 3894–3909, doi: 10.1002/hyp.13860, 2020.

Ji, F., Fan, L., Andrews, C. B., Yao, Y., & Zheng, C.: Dynamics of seasonally frozen ground in the Yarlung Zangbo River Basin on the Qinghai-Tibet Plateau: historical trend and future projection, Environmental Research Letters, 15, 104081, doi: 10.1088/1748-9326/abb731, 2020.

Juen I, Kaser G and Georges C.: Modelling observed and future runoff from a glacierized tropical catchment (Cordillera Blanca, Peru). Global and Planetary Change, 59(1-4): 37-48. doi: 10.1016/j.gloplacha.2006.11.038, 2007.

Kendall, M.G.: Rank Correlation Methods. 4th Edition, Charles Griffin, London, 1975.

Kirchner, J. W.: Catchments as simple dynamical systems: catchment characterization, rainfall-runoff modeling, and doing hydrology backward, Water Resources Research, 45, W02429, doi: 10.1029/2008WR006912, 2009.

Koch, J.C., C.P. Kikuchi, K.P. Wickland, and P. Schuster.: Runoff sources and flow paths in a partially burned, upland boreal catchment underlain by permafrost. Water Resources Research, 50:8141–8158. doi:10.1002/2014WR015586, 2014.

Lamontagne-Hallé, P., McKenzie, J. M., Kurylyk, B. L., and Zipper, S. C.: Changing groundwater discharge dynamics in permafrost regions, Environmental Research Letters, 13, 084017, doi: 10.1088/1748-9326/aad404, 2018.

Li, Z. J., Li, Z. X., Song, L. L., Ma, J. Z., and Song Y.: Environment significance and hydrochemical characteristics of suprapermafrost water in the source region of the Yangtze River, Science of The Total Environment, 644, 1141–1151, doi: 10.1016/j.scitotenv.2018.07.029, 2018.

Lin, Lu, Gao, Man, Liu, Jintao, Wang, Jiarong, et al.: Understanding the effects of climate warming on streamflow and active groundwater storage in an alpine catchment: the upper Lhasa river, Hydrology and Earth System Sciences, 24(3), 1145-1157. doi: 10.5194/hess-24-1145-2020, 2020.

Liu J P, Zhang W C.: Spatial variability in degree-day f actors in Yarlung Zangpo River Basin, China. Journal of University of Chinese Academy of Sciences. 35(5), 704-711. 2018.

Liu, Z., Yao, Z., Huang, H., Wu, S., & Liu, G.: Land use and climate changes and their impacts on Runoff in the Yarlung Zangpo River Basin, China, Land Degradation & Development, 25 (3) (2014), 203-215, doi: 10.1002/ldr.1159, 2014.

Lyon, S. W. and Destouni, G.: Changes in catchment-scale recession flow properties in response to permafrost thawing in the Yukon River basin, International Journal of Climatology, 30, 2138–2145, doi: 10.1002/joc.1993, 2010.

Lyon, S. W., Destouni, G., Giesler, R., Humborg, C., Mörth, M., Seibert, J., Karlsson, J., and Troch, P. A.: Estimation of permafrost thawing rates in a sub-arctic catchment using recession flow analysis, Hydrology and Earth System Sciences, 13, 595–604, doi: 10.5194/hess-13-595-2009, 2009.

Mallakpour, I., & Villarini, G.: A simulation study to examine the sensitivity of the Pettitt test to detect abrupt changes in mean. International Association of Scientific Hydrology Bulletin, 61(1–4), 245–254. doi: 10.1080/02626667.2015.1008482, 2016.

Mann, H.: Non-parametric test against trend, Econometrical, 13, 245–259, doi: 10.2307/1907187, 1945.

Mao Tianxu, Wang Genxu.: Analysis on characteristics of low-flow based on the monthly runoff recession coefficient in the Three-river headwaters region, Resources and environment in the Yangtze basin, 25(07): 1150-1157. doi: 10.11870/cjlyzyyhj201607018, (in Chinese) 2016.

Niu F.J., Gao, Z.Y. Lin, Z.J. Luo, J. Fan, X.W.: Vegetation influence on the soil hydrological regime in permafrost regions of the Qinghai-Tibet Plateau, China, Geoderma, 354, p. UNSP113892, doi: 10.1016/j.geoderma.2019.113892, 2019.

Payn, R. A., Gooseff, M. N., McGlynn, B. L., Bencala, K. E., & Wondzell, S. M.: Exploring changes in the spatial distribution of stream baseflow generation during a seasonal recession, Water Resources Research, 48(4), 519. doi:10.1029/2011WR011552, 2012.

Pepin, N., R.S. Bradley, H.F. Diaz, M. Baraer, E.B. Caceres, N. Forsythe, H. Fowler, et al.: Elevation dependent warming in mountain regions of the world. Nature Climate Change, 5:424–430, doi:10.1038/nclimate2563, 2015.

Pettitt, A. N.: A non-parametric approach to the change-point problem. Journal of the Royal Statistical Society, 28(2), 126–135, doi:10.2307/2346729, 1979.

Ren, W., Yao, T., Xie, S.: Stable isotopic composition reveals the spatial and temporal dynamics of discharge in the large river of Yarlungzangbo in the Tibetan Plateau, Science of The Total Environment, 625, 373–381, doi: 10.1016/j.scitotenv.2017.12.310, 2018.

Sen, P. K.: Estimates of the regression coefficient based on Kendall's tau, Journal of the American Statistical Association, 63(324), 1379–1389, doi:10.1080/01621459.1968.10480934, 1968.

Shi Dongping, Tan Hongbing, Chen Xi, Rao Wenbo, Renci Basang.: Uncovering the mechanisms of seasonal river–groundwater circulation using isotopes and water chemistry in the middle reaches of the Yarlungzangbo River, Tibet, Journal of Hydrology, 603, 127010, doi: 10.1016/j.jhydrol.2021.127010, 2021.

Su, F., Zhang, L., Ou, T., Chen, D., Yao, T., Tong, K., & Qi, Y.: Hydrological response to future climate changes for the major upstream river basins in the Tibetan Plateau. Global and Planetary Change, 136, 82–95, doi: 10.1016/j.gloplacha.2015.10.012, 2015.

Tallaksen, L. M.: A review of baseflow recession analysis. Journal of Hydrology, 165(1–4), 349–370, doi: 10.1016/0022-1694(94)02540-R, 1995.

Tan, Hongbin, Chen, Xi, Shi, Dongping, Rao, Wenbo, Liu, Jing, Liu, Jintao, Christopher J. Eastoe, Wang, Jiarong.: Base flow in the Yarlungzangbo River, Tibet, maintained by the isotopically-depleted precipitation and groundwater discharge. Science of The Total Environment, 759, 143510, doi: 10.1016/j.scitotenv.2020.143510, 2021.

Tashie, A. M., Scaife, C. I., & Band, L. E.: Transpiration and subsurface controls on streamflow recession characteristics. Hydrological Processes, 33(19), 2561–2575. https://doi.org/10.1002/hyp.13530, 2019.

Tashie, A., Pavelsky, T., & Emanuel, R. E.: Spatial and temporal patterns in baseflow recession in the continental United States, Water Resources Research, 55. doi: 10.1029/2019WR026425, 2020.

Tian, F., Xu, R., Nan, Y., Li, K., & He, Z.: Quantification of runoff components in the Yarlung Tsangpo River using a distributed hydrological model. Advances in Water Science, 31(03), 324–336, doi: 10.14042/j.cnki.32.1309.2020.03.002, (in Chinese) 2020.

Vuille M, Kaser G and Juen I.: Glacier mass balance variability in the Cordillera Blanca, Peru and its relationship with climate and the large-scale circulation. Global and Planetary Change 62(1-2): 14-28, doi: 10.1016/j.gloplacha.2007.11.003, 2008.

Walvoord, M. A. and Kurylyk, B. L.: Hydrologic impacts of thawing permafrost – A review, Vadose Zone Journal, 15, 1–20, doi: 10.2136/vzj2016.01.0010, 2016.

Walvoord, M. A. and Striegl, R. G.: Increased groundwater to stream discharge from permafrost thawing in the Yukon River basin: Potential impacts on lateral export of carbon and nitrogen, Geophysical Research Letters, 34, 123–134, doi: 10.1029/2007GL030216, 2007.

Walvoord, M. A., Voss, C. I., & Wellman, T. P.: Influence of permafrost distribution on groundwater flow in the context of climate-driven permafrost thaw: Example from Yukon Flats Basin, Alaska, USA. Water Resources Research, 48(7), 524. doi: 10.1029/2011WR011595, 2012.

Wang, Jiarong, Chen, Xi, Hu, Qi, & Liu, Jintao.: Responses of terrestrial water storage to climate variation in the Tibetan Plateau. Journal of Hydrology, 584, 124652. doi: 10.1016/j.jhydrol.2020.124652, 2020.

Wang, Jiarong, Chen, Xi, Liu, Jintao, & Hu, Qi.: Changes of precipitation-runoff relationship induced by climate variation in a large glaciated basin of the Tibetan Plateau. Journal of Geophysical Research: Atmospheres, 126, e2020JD034367. doi: 10.1029/2020JD034367, 2021.

Wang, Y. H., Yang, H. B., Gao, B., Wang, T. H., Qin, Y., and Yang, D. W.: Frozen ground degradation may reduce future runoff in the headwaters of an inland river on the northeastern Tibetan Plateau, Journal of Hydrology, 564, 1153–1164, doi: 10.1016/j.jhydrol.2018.07.078, 2018.

Wright, N., M. Hayashi, and W.L. Quinton.: Spatial and temporal variations in active layer thawing and their implication on run-off generation in peat-covered permafrost terrain. Water Resources Research, 45. doi:10.10129/2008WR006880, 2009.

Xu Xiaoming, Wu Qingbai, Zhang Zhongqiong.: Responses of active layer thickness on the Qinghai Tibet Plateau to climate change, Journal of Glaciology and Geocryology, 39(1): 1-8. doi: 10.7522/j.issn.1000-0240.2017.0001, (in Chinese) 2017.

Yamazaki, Y., J. Kubota, T. Ohata, V. Vuglinsky, and T. Mizuyama.: Seasonal changes in runoff characteristics on a permafrost watershed in the southern mountainous regions of eastern Siberia. Hydrological Processes, 20(3):453–467. doi:10.1002/hyp.5914, 2006.

Yang, K., & He, J.: China meteorological forcing dataset (1979-2018). National Tibetan Plateau Data Center [data set]. doi: 10.11888/AtmosphericPhysics.tpe.249369.file, 2019.

Yao, T. D., Pu, J. C., Lu, A. X., Wang, Y. Q., and Yu, W. S.: Recent glacial retreat and its impact on hydrological processes on the Tibetan Plateau, China, and surrounding regions, Arctic, Antarctic, and Alpine Research, 39, 642–650, doi: 10.1657/1523-0430(07-510)[YAO]2.0.CO;2, 2007.

Yao, T. D., Wang, Y. Q., Liu, S. Y., Pu, J. C., Shen, Y. P., and Lu, A. X.: Recent glacial retreat in high Asia in China and its impact on water resource in northwest China, Science in China Ser. D Earth Sciences, 47, 1065–1075, doi: 10.1360/03yd0256, 2004.

Yao, Y., Zheng, C., Andrews, C.B., Scanlon, B.R., Kuang, X., Zeng, Z., Jeong, S.-J., Lancia, M., Wu, Y., Li, G.: Role of groundwater in sustaining northern Himalayan rivers. Geophysical Research Letters, 48, e2020GL092354. doi: 10.1029/2020GL092354, 2021.

Yi, Wenxuan, Feng, Yuqing, Liang, Sihai, Kuang, Xingxing, Yan, Dezhao, & Wan, Li.: Increasing annual streamflow and groundwater storage in response to climate warming in the Yangtze river source region, Environmental Research Letters, 16(8), 084011, doi: 10.1088/1748-9326/ac0f27, 2021.

620 Yue, S., & Wang, C. Y.: Applicability of pre-whitening to eliminate the influence of serial correlation on the Mann-Kendall test, Water Resources Research, 38, doi:10.1029/2001WR000861, 2002.

Zhang, D., Huang, J., Guan, X., Chen, B., & Zhang, L.: Long-term trends of perceptible water and precipitation over the Tibetan Plateau derived from satellite and surface measurements, Journal of Quantitative Spectroscopy & Radiative Transfer, 122, 64–71, doi: 10.1016/j.jqsrt.2012.11.028, 2013.

Table 1. Information of the data used in this study.

Data	Period	Spatial-Resolution	Temporal-Resolution	Source
Precipitation (P, mm) Mean Temperature (T, ℃) Evapotranspiration (E, mm) Discharge (Q, mm)	1980~2015	0.1°×0.1° Obs. stations	Daily Daily	National Tibetan Plateau Data Center; http://data.tpdc.ac.cn http://data.cma.cn
NDVI	1982-2015	1/12°×1/12°	15-days	http://data.tpdc.ac.cn
Glacial area	1976, 2000, 2013	30m×30m	Annual	http://data.tpdc.ac.cn and China's second glacier catalogue data
	2006~2011 (in 2009)		Mean annual	
Permafrost and Frozen ground	1983-1996, 1997, 2003, 2012, 2017	1km×1km	Mean annual	http://data.tpdc.ac.cn
Active layer thickness (ALT)	1980-2015	0.1°×0.1°	Annual	Calculated by a linear function from Xu et al. (2017)

Table 2. Summary of sub-basin characteristics in YR basin.

Regions		NGS	YC	NX	YBJ	LS
Drainage area (10^4 km^2)		10.86	16.51	20.32	0.31	3.06
Mean Elevation (m asl)		3776	3553	2944	4255	3794
Glacier area (km^2)	(year) 1976	2070	2902	4285	241	283
	2001	1822	2562	3821	227	257
	2009*	1674	2355	3782	224	255
	2013	1489	2217	3709	220	247
Percentage of permafrost area (%, 2003)		47.7	44.1	41.8	44.9	44.5
Mean annual value	*P* (mm)	354	386	426	433	536
	T (^{0}C)	-1.51	-1.16	-0.99	-2.15	-1.91
	T_{re} (^{0}C)	-6.23	-5.95	-5.73	-8.37	-6.83
	Q (mm)	144	180	290	240	302
	Q_{re} (mm)	26.5	34.0	52.3	31.5	47.9
	Rc (R/P)	0.410	0.460	0.680	0.555	0.563
	CV_1	1.099	1.061	0.931	1.138	1.123
	CV_2	1.155	1.070	0.970	1.106	1.203

* Glacier area is from China's second glacier catalogue data in 2009. The mean of A_{ice} in year 1976 and 2001 is used as a reference value in the sub-period before 1997, and the mean of A_{ice} in 2001, 2009, and 2013 is used as a reference value in the sub-period after 1997. The subscript "1", and "2" represent 1980-1996, and 1997-2015, respectively.

Table 3. Mean values of parameters a (mm^{1-b} d^{b-2}), a' (d^{-1}) and b (dimensionless), recession coefficient K (mm^{b-1} d^{2-b}), and recession timescale τ (d). * indicates significant by TFPW-MK test ($p< 0.05$). Values in brackets refer to the range of annual value.

Period	Index	Mean annual value				
		NGS	YC	NX	YBJ	LS
1980–2015	a	0.042 (0.033~0.060)	0.032 (0.025~0.043)	0.022 (0.019~0.027)	0.038 (0.025~0.052)	0.024 (0.018~0.032)
1980–1996		0.046	0.035	0.023	0.043	0.022
1997–2015		0.039	0.029	0.021	0.034	0.025
	Δa	**-0.007***	**-0.006***	**-0.002***	**-0.009***	**0.003***
1980–2015	a'	0.015 (0.011~0.025)	0.015 (0.011~0.025)	0.017 (0.013~0.022)	0.025 (0.015~0.043)	0.017 (0.012~0.022)
1980–1996		0.017	0.017	0.019	0.027	0.015
1997–2015		0.014	0.014	0.015	0.023	0.017
	$\Delta a'$	**-0.003***	**-0.003***	**-0.004***	**-0.004***	**0.002***
1980–2015	b	1.85 (1.645~1.990)	1.70 (1.506~1.992)	1.54 (1.297~1.789)	1.85 (1.607~1.979)	1.36 (1.117~1.783)
1980–1996		1.81	1.67	1.48	1.78	1.25
1997–2015		1.89	1.73	1.59	1.90	1.47
	Δb	**0.08***	**0.06**	**0.11***	**0.11***	**0.22***
1980–2015	K	129.7 (73.7~196.5)	127.3 (68.3~203.0)	97.9 (63.4~131.0)	142.9 (59.0~205.4)	64.2 (46.3~88.8)
1980–1996		100.9	94.0	86.6	98.9	58.0
1997–2015		155.5	157.5	107.6	172.1	69.5
	ΔK	**54.6***	**63.5***	**21.0***	**73.2***	**11.5***
1980–2015	τ	90.8 (65.7~117.3)	89.7 (64.0~126.6)	75.3 (56.7~108.4)	93.0 (56.1~141.7)	65.0 (49.0~110.9)
1980–1996		88.2	83.1	71.7	77.8	57.3
1997–2015		93.4	96.4	78.8	98.5	71.8
	$\Delta\tau$	**5.2**	**13.4***	**7.1**	**20.7***	**14.5***

Table 4. The storage sensitivity of discharge (λ_S, mm^{-1}), and sensitivity coefficients of recession parameters of a' ($\lambda_{a'}$) and b (λ_b), T (λ_T) and Q (λ_Q) to storage change (ΔS) during different periods for each sub-basin. The values in the bracket refer to the range of annual value.

Period	Index	Mean annual value				
		NGS	YC	NX	YBJ	LS
1980–2015	λ_S	0.059 (0.035~0.095)	0.048 (0.030~0.090)	0.036 (0.026~0.058)	0.053 (0.032~0.095)	0.050 (0.035~0.085)
1980–1996		0.069	0.058	0.042	0.066	0.056
1997–2015		0.050	0.042	0.031	0.041	0.046
	$\Delta\lambda_S$	**-0.019***	**-0.016***	**-0.012***	**-0.025***	**-0.010**
1980–2015	$\lambda_{a'}$	-1380	-2131	-2920	-2051	-1733
1980–1996		-948	-1291	-2177	-1247	-1595
1997–2015		-1984	-3538	-3822	-3777	-1927
	$\Delta\lambda_{a'}$	**-1036***	**-2274***	**-1645***	**-2530***	**-332**
1980–2015	λ_b	664	477	204	786	96
1980–1996		435	270	157	371	72
1997–2015		950	786	257	1428	129
	$\Delta\lambda_b$	**515***	**515***	**100***	**1057***	**58**
1980–2015	λ_Q	90.8	89.7	75.3	93.0	65.0
1980–1996		88.2	83.1	71.7	77.8	57.3
1997–2015		93.4	96.4	78.8	98.5	71.8
	$\Delta\lambda_Q$	**5.2**	**13.4***	**7.1**	**20.7***	**14.5***
1980–2015	λ_T	37.1	51.0	25.1	95.2	11.9
1980–1996		24.4	28.8	18.8	46.7	7.2
1997–2015		52.5	83.8	32.4	163.5	18.8
	$\Delta\lambda_T$	**28.1***	**55.1***	**13.6**	**111.3***	**11.7**

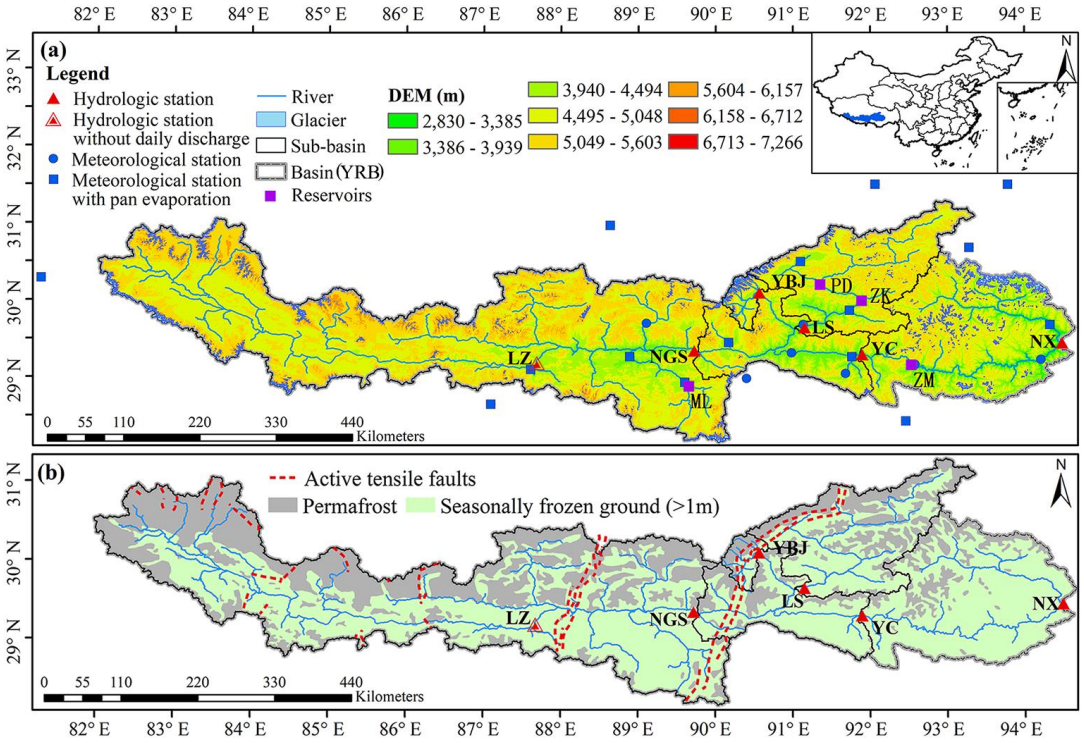

Figure 1. (a) Geographical location of the Yarlung-Zangpo River basin (YRB, the entire basin above the hydrological station of NX) and its five sub-basins (NGS, YC, NX, YBJ, and LS) from upstream to downstream (NGS for Nugesha, YC for Yangcun, NX for Nuxia, YBJ for Yangbajain, and LS for Lhasa). (b) Distributions of permafrost and seasonally frozen ground in 2012 and active tensile faults (the red dotted lines).

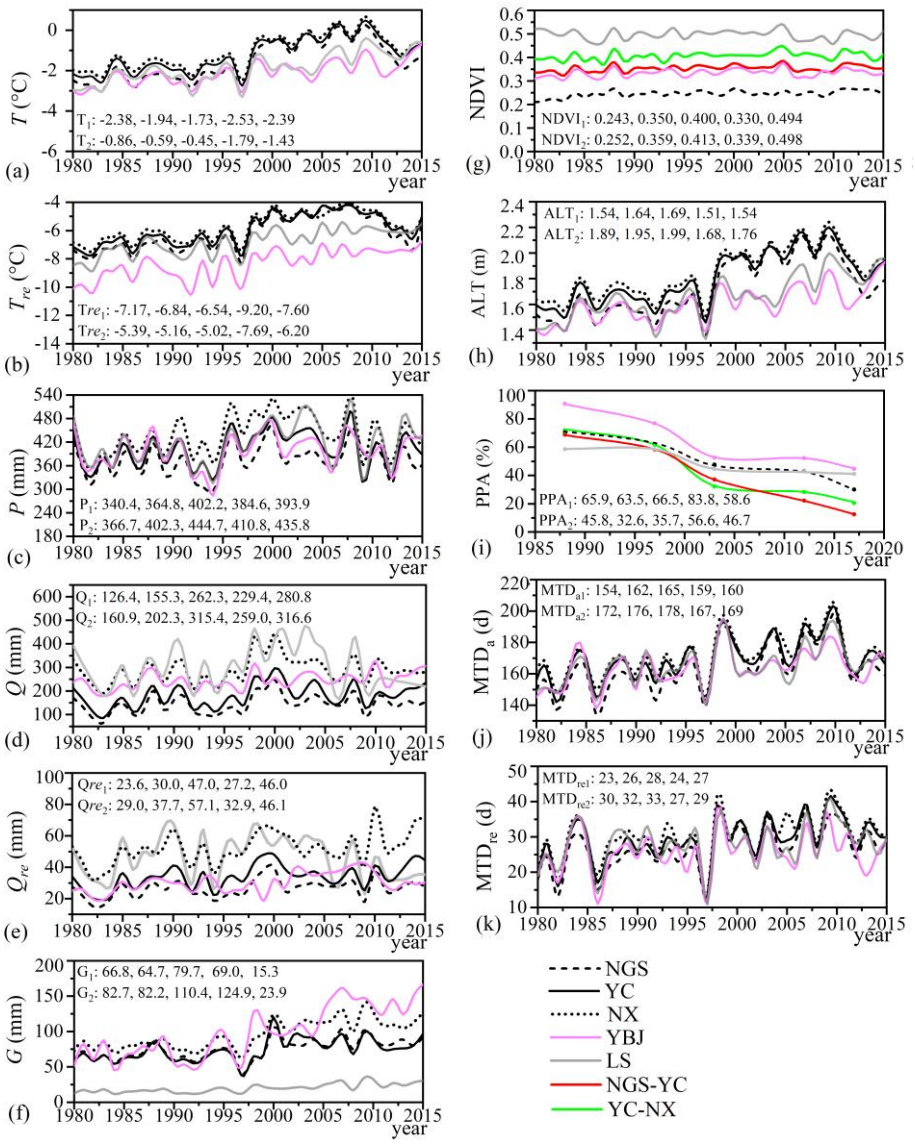

Figure 2. Variations of (a) annul mean temperature (*T*), (b) mean temperature in recession period (T_{re}), (c) precipitation (*P*), (d) discharge (*Q*), (e) discharge in recession period (Q_{re}), (f) glacier meltwater (*G*), (g) NDVI, (h) active layer thickness (ALT), (i) percentage of permafrost area (PPA), (j) the total number of days with the mean temperature above 0 ℃ in a year (MTD_a), and (k) the total number of days with the mean temperature above 0 ℃ for recession period (MTD_{re}) from 1980 to 2015 in the five sub-basins. The subscripts "1" and "2" refer to the early period from 1980 to 1996 and the recent period from 1997 to 2015, respectively. NGS-YC refers to the area between the nested sub-basins NGS and YC, and YC-NX is for the area of the nested sub-basins YC and NX.

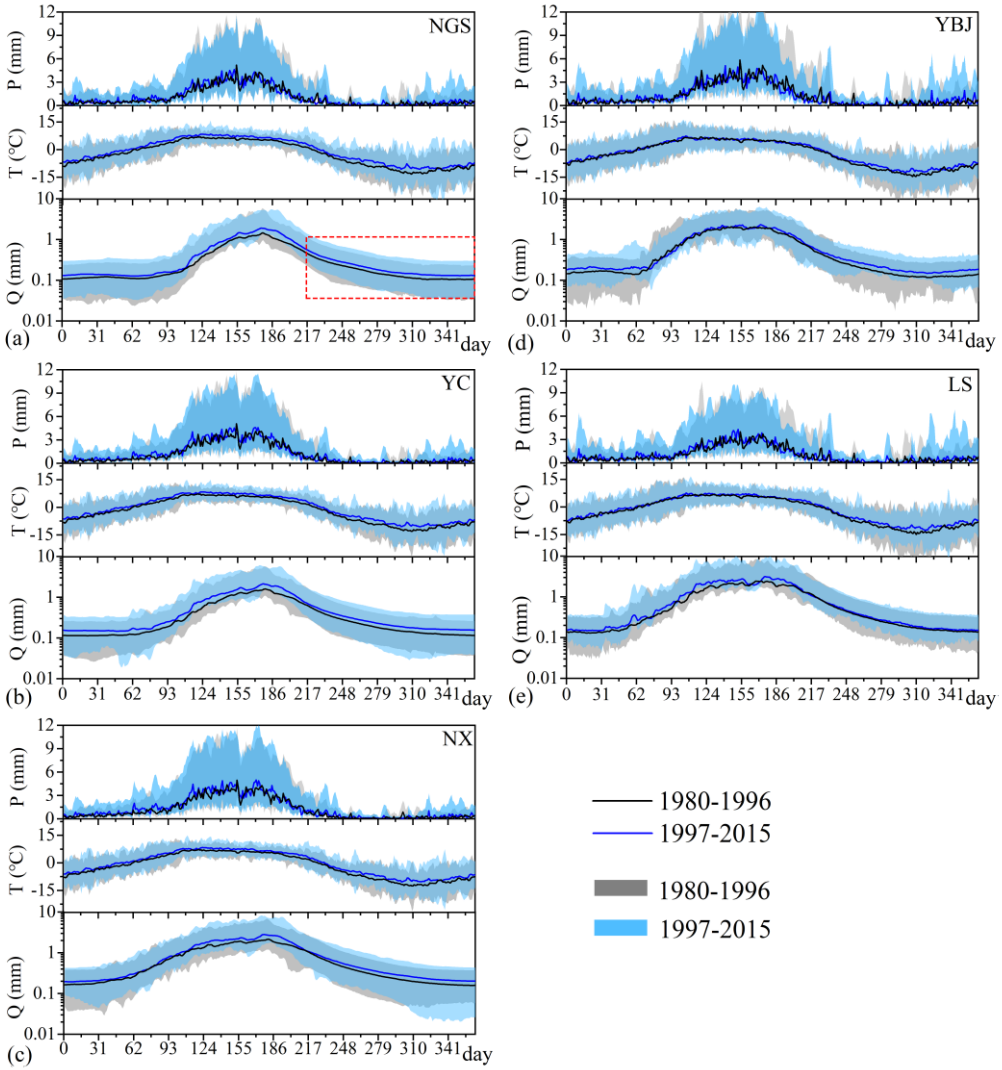

655 **Figure 3.** (a)-(e): *P*, *T*, and *Q* in a hydrological year (from 1 March to 28 February of the following year) for the two periods in the five sub-basins. The red dashed rectangle in (a) shows the hydrograph recession from 1 October to 15 February of the following year, and the shading shows the range of the daily variation of *P*, *T*, and *Q* in each period.

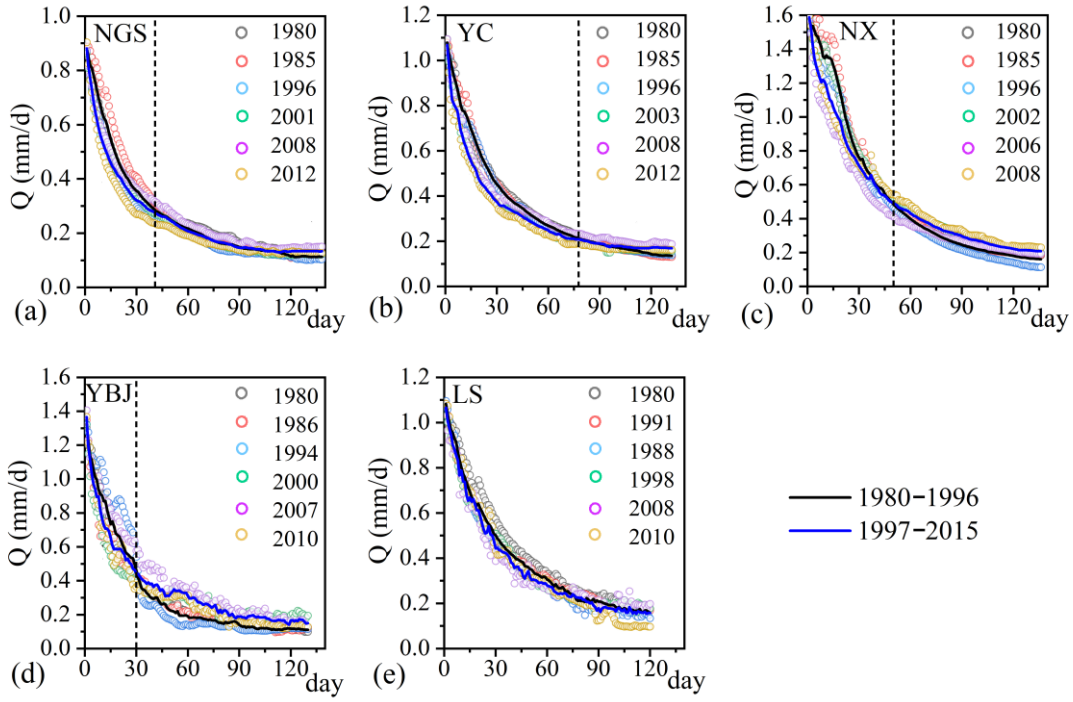

Figure 4. Discharge recession for selected years with approximately the same initial discharge Q_0 in each sub-basin.

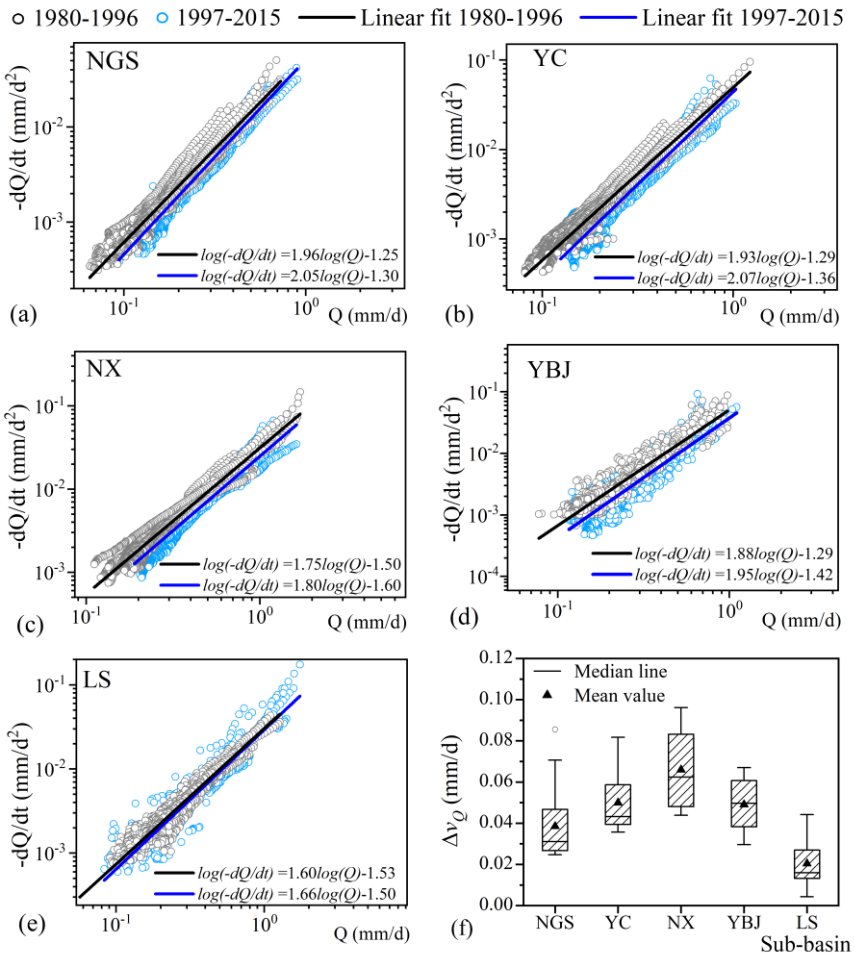

660

Figure 5. (a)-(e): Plot of -dQ/dt vs. Q in log-log diagram for each recession hydrograph during 1980–2015, and the fitting lines [log(-dQ/dt) = $b$log(Q)+log(a)] for the data points in the two periods for the five sub-basins. (f): Differences of mean recession rates between the two periods (Δv_Q) estimated from the non-overlapping moving averages of the 5-days' series.

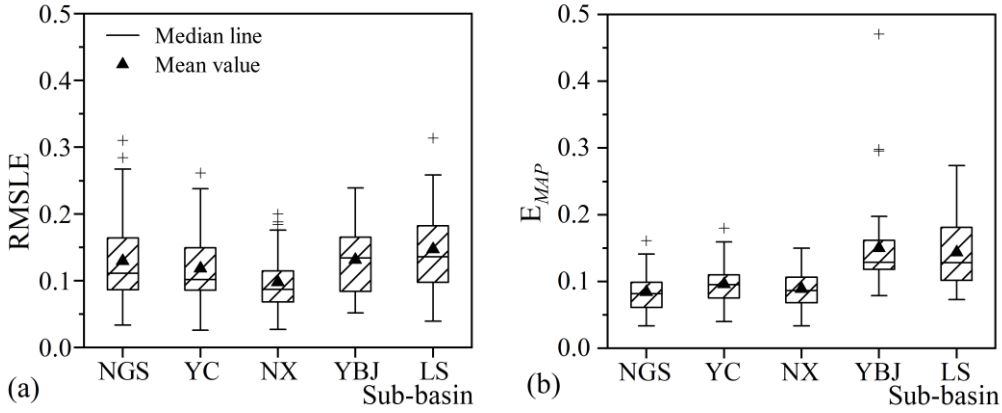

665

Figure 6. The Box-plot of (a) RMSLE of -d*Q*/d*t* between observed and estimated discharge; and (b) E_{MAP} between annual mean observed and estimated discharge for individual recession hydrographs in each sub-basin.

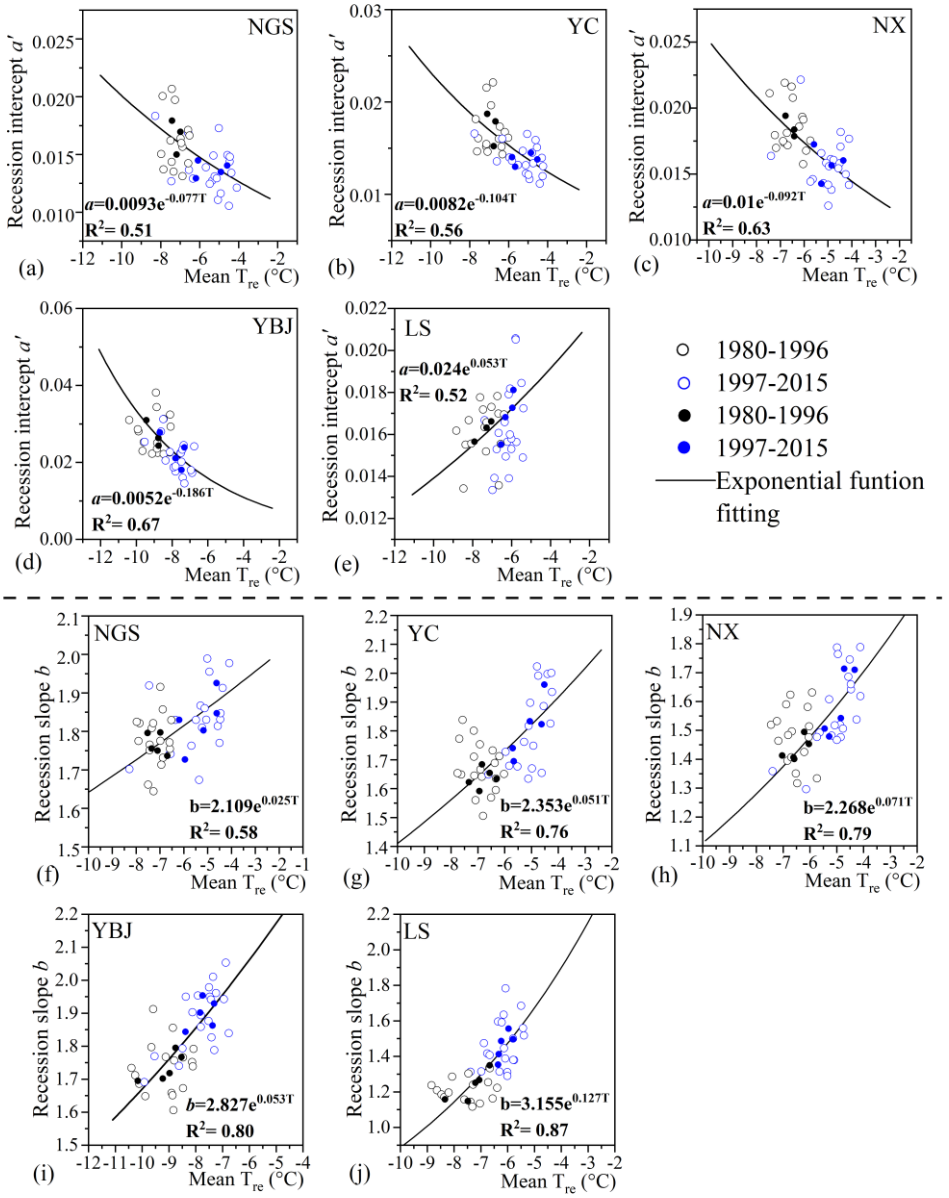

Figure 7. (a)-(e): The exponential function of a' with T_{re} for each sub-basin. (f)-(j): Same as (a)-(e) but for recession slope b. The solid and open circles represent 4-year average and annual value, respectively.

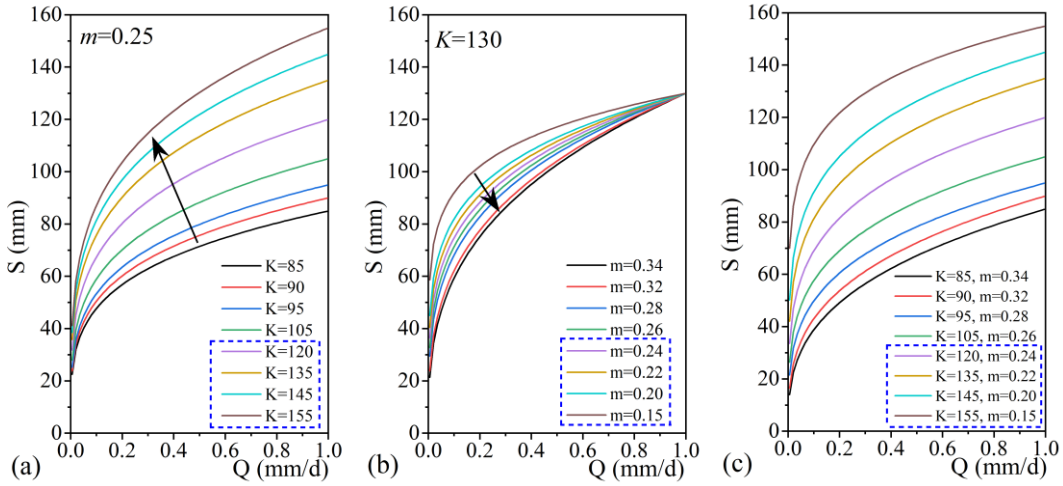

Figure 8. Relationship of *S* and *Q* at different values of *K* (a) and *m* (b), and combinations of *K* and *m* (c) in the two periods for sub-basin YC. The different set of numbers in the blue dashed line box in each panel shows the *K* and *m* values and therefore different *S*–*Q* relationships in the recent warmer period.

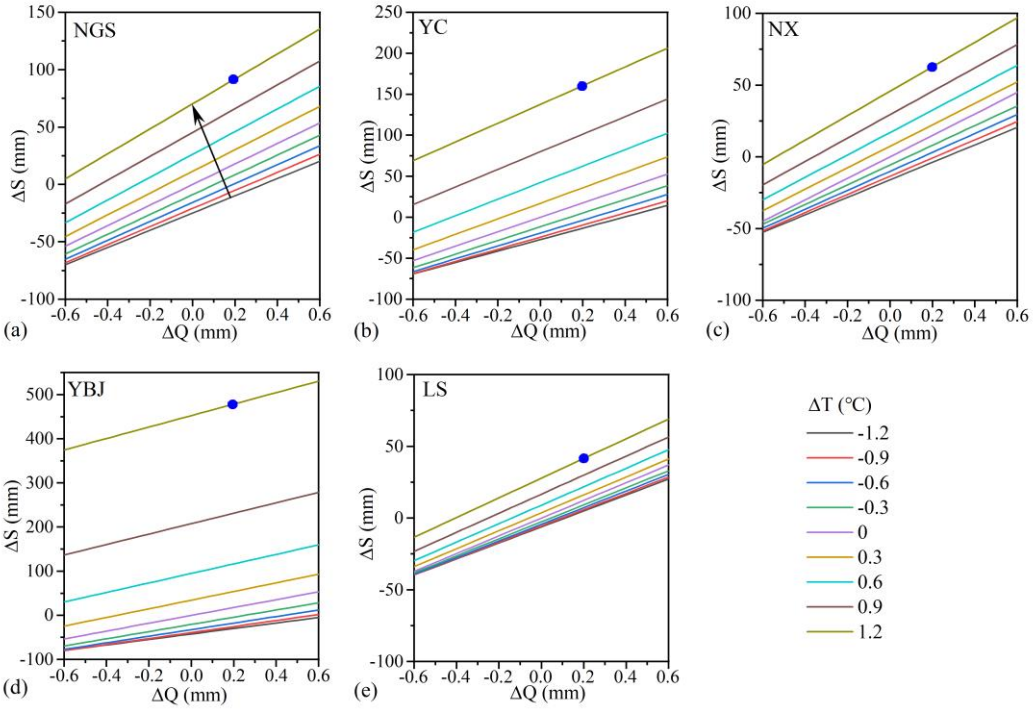

675

Figure 9. Changes in storage Δ*S* in relation to changes in discharge Δ*Q* under different changes in temperature Δ*T* for each sub-basin. The changes in temperature Δ*T* refer to annual values relative to mean annual temperature in the recession period during 1980–2015. The solid circle refers the point of Δ*S* in response to 0.2mm of Δ*Q*.

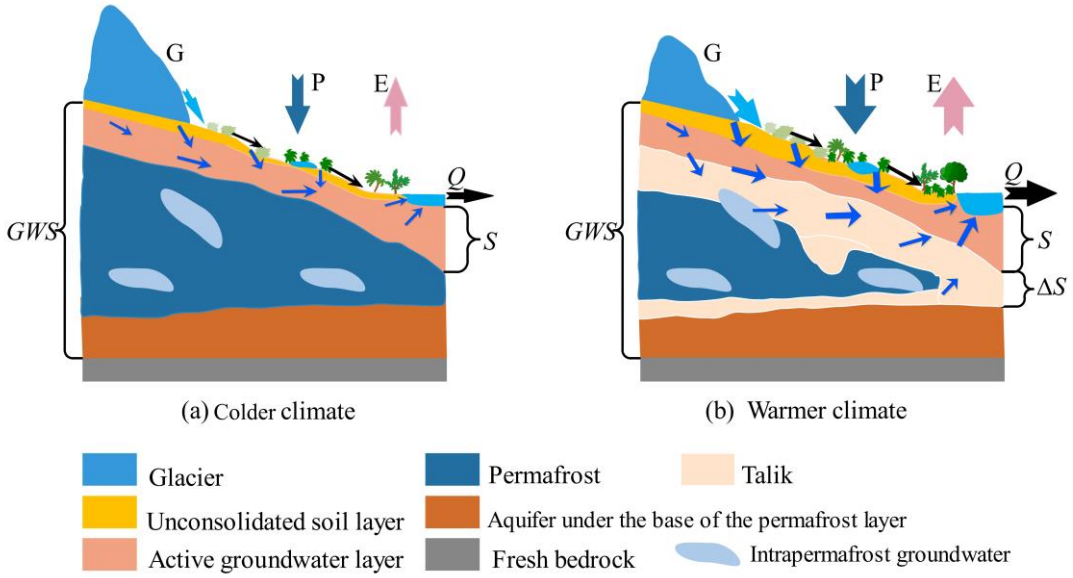

680 **Figure 10.** A schematic illustration of climate warming effect on surface conditions and subsurface profile as well as hydrological variables. The larger sizes of the arrows indicate a large increase of the hydrological variables, e.g., glacier melting, precipitation, discharge, and evaporation.